Aging-associated and CD4 T-cell–dependent ectopic CXCL13 activation predisposes to anti–PD-1 therapy-induced adverse events

AUTHOR(S):

Tsukamoto, Hirotake; Komohara, Yoshihiro; Tomita, Yusuke; Miura, Yuji; Motoshima, Takanobu; Imamura, Kosuke; Kimura, Toshiki; ... Kamba, Tomomi; Sakagami, Takuro; Oshiumi, Hiroyuki

CITATION:

Tsukamoto, Hirotake ...[et al]. Aging-associated and CD4 T-cell–dependent ectopic CXCL13 activation predisposes to anti–PD-1 therapy-induced adverse events. Proceedings of the National Academy of Sciences (PNAS) 2022, 119(29): e2205378119.

ISSUE DATE:

2022-07-19

URL:

http://hdl.handle.net/2433/274899

京都大学 KYOTO UNIVERSITY
PNAS
RESEARCH ARTICLE | IMMUNOLOGY AND INFLAMMATION
OPEN ACCESS

Aging-associated and CD4 T-cell–dependent ectopic CXCL13 activation predisposes to anti–PD-1 therapy-induced adverse events

Hirotake Tsukamoto[a,b,1], Yoshihiro Komohara[c], Yusuke Tomita[d], Yuji Miura[c,e], Takanobu Motoshima[f], Kosuke Imamura[d], Toshiki Kimura[d], Tokunori Ikeda[g], Yukio Fujiwara[c], Hiromu Yano[c], Tomomi Kamba[f], Takuro Sakagami[d], and Hiroyuki Oshiumi[b]

Edited by Tyler Curiel, Dartmouth College, Hanover, NH; received March 30, 2022; accepted May 20, 2022 by Editorial Board Member Philippa Marrack

Clinical success of immune-checkpoint blockade (ICB) cancer immunotherapy is compromised by increased risk of immune-related adverse events (irAEs). However, mechanistic action(s) of immune responses underlying development of irAE remain not fully explored. Here, we found that in tumor-bearing aged, but not young, mice, antiprogrammed death receptor (PD)-1 therapy elicited irAE-like multiorgan dysfunctions with ectopic accumulation of T and B cells in damaged organs. In this preclinical model, the organ toxicities were mediated by immunoglobulin G (IgG) deposition because administration of IG from ICB-treated aged mice induced the pathogenicity specifically in naïve aged hosts. Mechanistically, CD4 T-cell–derived interleukin (IL)-21 upregulated B-cell–homing chemokine, CXCL13, preferentially in irAE organs from aged mice treated with anti–PD-1 therapy. The ICB-induced pathogenicity was alleviated by B-cell depletion or by blockade of IL-21 or CXCL13 activity. These results suggest that age-associated immune regulatory milieu contributes to the formation of tertiary lymphoid structure-like lymphocytic aggregates in irAE organs and irAE-related toxicity employing IL-21-CXCL13-auto-antibody axis. Supporting this, a systemic increase in CXCL13 and *Il21* expression in CD4 T cells correlated with irAE incidence in ICB-treated patients. These findings provide rationale for therapeutic usefulness of CXCL13 in irAE management.

Significance

Immune-related adverse events (irAEs) induced by immune-checkpoint blockade including antiprogrammed death receptor (PD)-1 therapy are a major problematic issue in cancer immunotherapy. Preclinical models for more physiologically occurring irAEs are potentially useful for the clarification of fundamental causes and natural developmental course of irAEs. Here, we found that in tumor-bearing aged, but not young, mice, anti–PD-(L)1 therapy alone induces irAE-like multiorgan toxicities through CD4 T-cell–derived interleukin (IL)-21 and subsequent age-specific CXCL13 expression in tertiary lymphoid structure. Consistent with this animal model, a systemic increase in CXCL13 correlates with irAE incidence in cancer patients. These findings provide insight into the development of management strategies for irAE that balance both irAE-related immune response and antitumor immune surveillance.

Immune-checkpoint blockade (ICB) with antiprogrammed death receptor (PD)-1/PD-L1 antibodies (Abs) is a common immunotherapeutic approach that has provided better outcomes with durable antitumor effects in a certain population of cancer patients (1–3). However, due to the critical role of PD-1/PD-L1 in maintaining self-tolerance (4), the clinical benefits may be hindered by a remarkable spectrum of therapy-associated organ toxicities, referred to as immune-related adverse events (irAEs) (5, 6). In non–small-cell lung carcinoma (NSCLC), more than 20% of patients treated with anti–PD-1 therapy developed serious irAEs of grades 3 to 5 (1), and of these, half of the patients who had discontinued the treatment due to the severe irAE recurred the initial or newly developed irAE when retreated with ICB (7). Moreover, in combination with other ICBs, anticytotoxic T lymphocyte-associated protein 4 (CTLA-4) Ab was shown to trigger severe irAEs in ∼60% of melanoma patients who experienced multiorgan toxicities, including pneumonitis, colitis, hepatitis, and thyroiditis (2, 3, 6). Consequently, patients with serious irAEs are permanently required to discontinue the ICB treatment regardless of its substantial antitumor effects (3, 5, 8). To minimize toxicity, a large proportion of patients with irAEs are managed with typical corticosteroids (2, 8). However, systemic immunosuppression via their high doses and/or long-lasting administration may also blunt antitumor immune response (9, 10). Therefore, irAEs are considered to be a major treatment-associated hindrance that limit further development of ICB-based cancer immunotherapy.

Due to a substantial number of irAE patients, most relevant knowledge on irAEs comes from human clinical research, which suggests the involvement of dysregulated immune tolerance against autoantigens (11, 12), pathogenic B-cell activation and subsequent auto-Ab production (12, 13), and T-cell reactivity preferentially associated with some major histocompatibility complex haplotypes (14, 15). Although autoimmunity-prone mice were reported and tested as experimental models for irAEs (5, 16), the mechanisms underlying spontaneous development of autoimmune-like irAE symptoms remain poorly understood. To identify therapeutic targets and to develop strategies for mitigating the occurrence of severe irAEs, animal models that recapitulate pathophysiologic process are urgently required. The properly developed irAE model helps design ways to prevent occurrences of irAEs and to maximize clinical use and benefits of ICBs without irAEs.

This article is a PNAS Direct Submission. T.C. is a guest editor invited by the Editorial Board.

[1]To whom correspondence may be addressed. Email: tsukamoto.hirotake.4j@kyoto-u.ac.jp.

This article contains supporting information online at http://www.pnas.org/lookup/suppl/doi:10.1073/pnas.2205378119/-/DCSupplemental.

Published July 11, 2022.

As elderly people represent the largest cohort of patients with cancer (17, 18), the number of older patients deemed eligible for ICBs is increasing. Although ICBs are reported to be effective in patients with melanoma regardless of their actual ages (19), some studies reported that the patients with irAEs were relatively older (20, 21). Indeed, the occurrences of some particular types of irAEs such as pneumonitis, hepatitis, arthritis, and thyroiditis have been reported to increase in older patients (19, 21). However, there is a gap in tolerability of ICBs between preclinical studies using young animals and real cancer patients. To bridge this gap, the present study investigated the tolerability of ICBs in older mice relative to their younger counterparts. Our findings describe previously uncharacterized multiorgan pathogenicity in tumor-bearing aged mice when treated with anti–PD-1 therapy. This irAE model allowed us to investigate its pathophysiological mechanisms and provided suggestive evidence that preferential activation of interleukin (IL)-21–producing CD4 T cells exacerbated anti–PD-1 therapy-induced pathologies through direct action to produce CXCL13 within irAE-affected organs.

Results

Anti–PD-1 Therapy-Induced irAE-Like Multiorgan Failures in Aged Mice. We found that ICBs with anti–PD-1/PD-L1 Abs were less effective for tumor eradication in aged mice orthotopically inoculated with ovalbumin (OVA)-expressing melanoma cells, MO4 (Fig. 1*A*). Tumor outgrowth in young mice was substantially attenuated by the treatment (22), as evidenced by the lower levels of lactate dehydrogenase, a poor prognostic factor (23) (Fig. 1*B*). These were consistent with previous reports with different models (24, 25). On the other hand, the treatment of aged mice with ICBs significantly increased levels of serologic clinical parameters indicative of organ dysfunctions: alanine aminotransferase (ALT)/triglyceride/total protein, amylase, and urea nitrogen/ureic acid (the biochemical markers for hepatitis, pancreatitis, and kidney failure, respectively; ref. 6). Moreover, in aged mice, we also observed elevated serum levels of surfactant protein D (SP-D), a clinical sign of exaggerated alveolar-capillary leakage from the alveolar space attributed to lung injury in interstitial pneumonia (26, 27). Notably, the levels of these toxicity-associated serologic markers were not altered by ICBs in tumor-bearing young mice or by control Ab injection in aged mice (Fig. 1*B*).

Consistent with the increase in serologic parameters, multiple organs including lung, kidney, and liver from ICB-treated aged mice, but not from their younger counterparts, showed ectopic dense aggregates of lymphocytes like tertiary lymphoid structures (TLSs) (28, 29) in peribronchial and perivascular interstitial regions (Fig. 1*C*), similar to what has been seen in irAE patients (6). Immunohistochemical (IHC) analysis revealed these TLSs consisted of B and T cells (Fig. 1 *D* and *F*). Tissue-infiltrating lymphocytes were quantified by removal of blood-circulating cells stained via intravenous injection of anti-CD45 Ab, indicating a four- to fivefold overall increase in the frequencies of CD4 and CD8 T cells in lung from ICB-treated aged mice (Fig. 1*F* and *SI Appendix*, Fig. S1 A and B). A significant increase in B-cell infiltration in lung and liver of these mice confirmed the histological cellular composition (*SI Appendix*, Fig. S1 *C* and *D*). In contrast, the frequencies of these populations in spleen were not changed, regardless of the treatment (Fig. 1*F*). As shown in Fig. 1 *D*–*F*, in vivo depletion of CD4 T cells with anti-CD4 Ab abolished multifocal TLS organization and significantly reduced lymphocytic infiltrations in ICB-treated aged mice.

Increased expression *of Il6* and *Il1a*, indicative of accelerated inflammatory response (22, 30), was also observed in the lungs of treated aged mice (*SI Appendix*, Fig. S1*E*). No significant changes in those factors were detected in isotype-matched control Ab-treated aged mice, excluding a possibility of immunogenic reaction against repeated administration of xenogeneic rat immunoglobulin G (IgG) (31). All animals did not result in fatality immediately after Ab administration and reached tumor-endpoint–related survival, indicating no anaphylactic responses. Aged C57BL/6 and Balb/c mice inoculated with other tumor cells, such as MC38 or CT26, also suffered from similar lymphocytic aggregates during the same regimen (*SI Appendix*, Fig. S1 *F* and *G*). These data indicate a general phenomenon specifically associated with ICB-treated aged mice, irrespective of tumor type or genetic background. Cumulatively, aged mice receiving anti–PD-(L)1 therapy can be utilized as an experimental model for investigation of the mechanism underlying irAE development.

Ab-Dependent Organ Toxicity Elicited by Anti–PD-1 Therapy in Aged Mice. In addition to the increase in several markers of organ dysfunctions, we found elevated levels of blood-circulating Ig in aged mice in response to ICB (Fig. 2*A*). Ab-mediated autoimmune pathogenicity has been reported to correlate with an increase in TLS (29). Consequently, we examined the effect of Ab response on ICB-mediated lung pathology and observed intense deposits of mouse IgG in the lung from aged, but not from young, mice treated with ICB (Fig. 2 *B* and *C*). This ICB-induced IgG deposition was reversed by CD4 depletion, but not by IL-6 deficiency, thereby supporting the critical role of CD4 T cells in the aberrant Ab response. This CD4 T-cell-dependent formation of lung lesions correlated with a systemic increase in serum SP-D levels (Fig. 2*D*), while IL-6 deficiency in aged mice did not improve the focal increases in lung lesion (*SI Appendix*, Fig. S2*A*). Consistent with the patients treated with combined administration of anti–PD-1 and anti–CTLA-4 Abs (3), additional CTLA-4 blockade significantly exacerbated irAE symptoms, indicated by increases in SP-D, ALT, and urea nitrogen in aged mice (*SI Appendix*, Fig. S2*B*). These exacerbated symptoms were accompanied by the systemically increased levels of IgG (*SI Appendix*, Fig. S2*B*) and lymphocytic infiltration (*SI Appendix*, Fig. S2 *C*–*E*), whereas anti–CTLA-4 therapy alone did not provide obvious effects on these events.

We further directly assessed potential aggravating effects of ICB on mechanical properties of lung using invasive lung damage testing. In tumor-bearing young mice, anti–PD-1 therapy had only minor effects on functional parameters of the lung, airway resistance, and pulmonary compliance/elastance (32) (Fig. 2*E*). However, ICB treatment in aged mice significantly increased the airway resistance and decreased the pulmonary compliance, indicating the deterioration of mechanical properties of airway and lung tissue, respectively. These observations were supported by an increased ratio of wet-to-dry lung tissue weight (*SI Appendix*, Fig. S2*F*), a surrogate indicator of lung dysfunction (33). As expected, CD4 depletion ameliorated such mechanical abnormalities (Fig. 2 *E* and *F*), strongly suggesting that ICB-induced lung dysfunction was governed by CD4 T-cell activation.

We next examined whether in vivo transfer of mouse IgG purified from serum of ICB-treated aged mice mimicked ICB-induced toxicity in naïve mice. Lung and kidney damages with elevated levels of SP-D and urea nitrogen, respectively, were induced only when aged mice-derived serum was transferred into

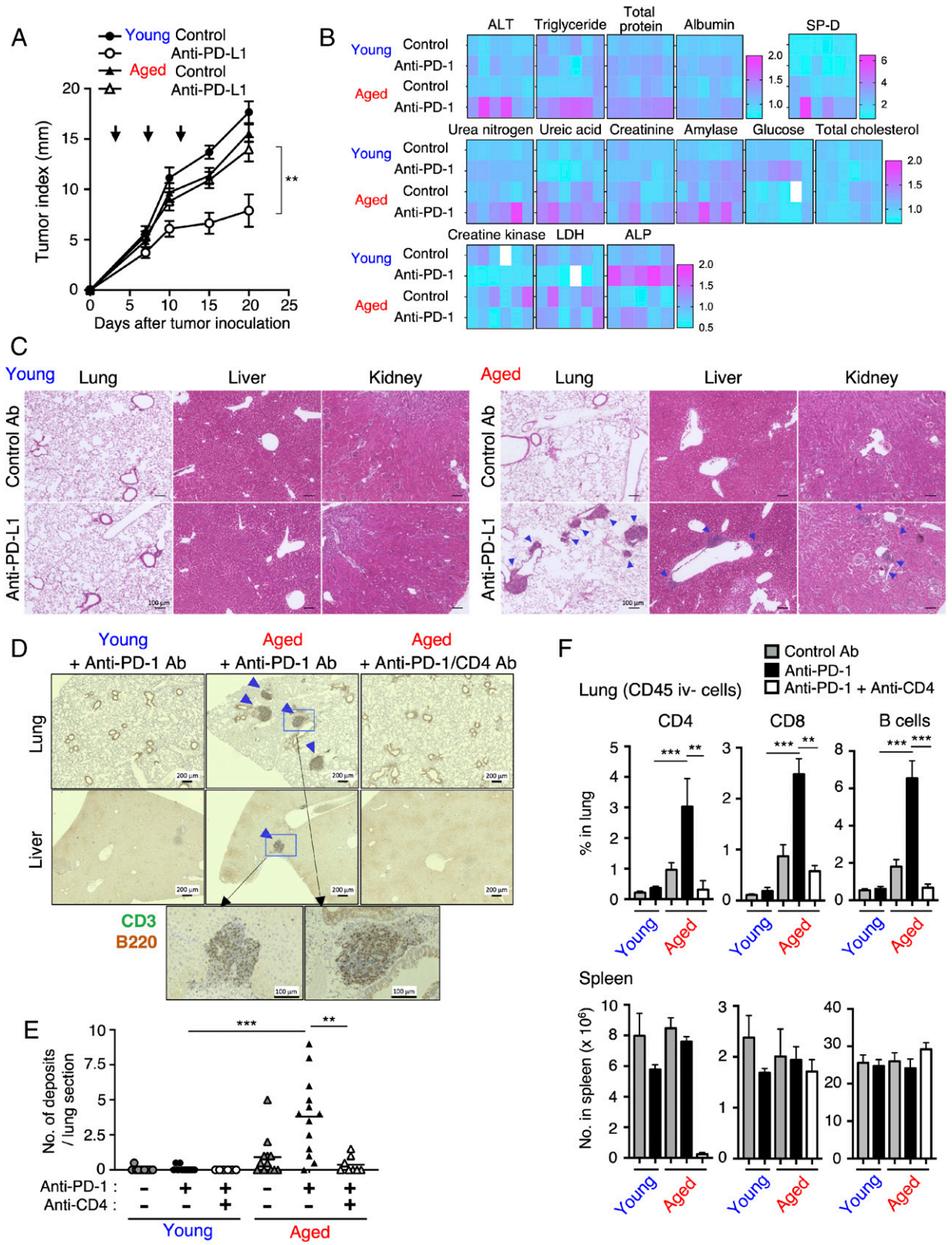

Fig. 1. Anti–PD-1 therapy induces multiorgan failures and aberrant lymphocytic accumulation in aged, but not in young, mice. MO4-bearing young or aged mice were treated with anti–PD-(L)1 Ab three times (indicated by arrows). (*A*) Tumor outgrowth was monitored with time. (*B*) Blood clinical markers of several organ dysfunctions were assessed in young and aged mice. Fold changes of each value for indicated conditions were calculated using average values in control Ab-treated young mice as 1 (shown as heatmaps). (*C* and *D*) H&E staining (*C*) and CD3 and B220 staining (*D*) in lung, liver, and kidney. (*E*) The number of ectopic lymphoid structures in each lung section ($n = 13$). (*F*) Frequencies of lung-infiltrating CD45 (iv)− CD4+, CD8+, and B220+ cells (*Top*) and splenic T and B cells (*Bottom*) were assessed in mice treated with indicated Abs. (Scale bars: 100 [*C*] and 200 [*D*] μm.) Data are represented as mean ± SEM. One-way ANOVA with Turkey post hoc test was used; $*P < 0.05$, $**P < 0.01$, $***P < 0.001$.

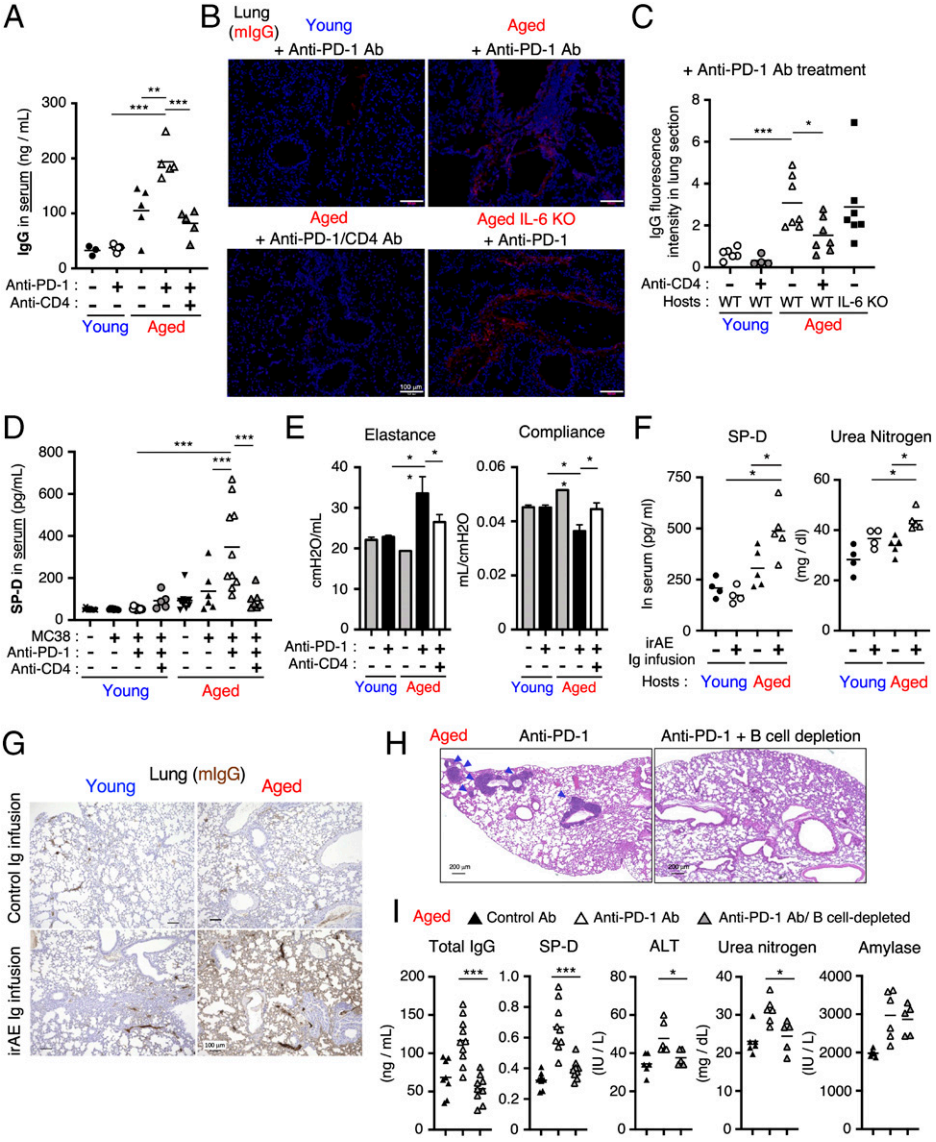

Fig. 2. Ab response is associated with irAE-related organ toxicity. (*A–F*) MC38-bearing young or aged mice were administrated with anti–PD-1 Abs together with CD4 depletion. (*A*) The concentration of Ig in blood (n = 3–5). Representative lung sections stained with anti-mouse IgG indicating (*B*) Ig deposition (red) and (*C*) their fluorescent intensities (per square millimeter lung area) (n = 6–7). (*D*) The concentration of SP-D released in blood (n = 6–10). (*E*) Lung dysfunction was assessed by mechanistic ventilation system (n = 5). (*F* and *G*) Irrelevant mouse IgG or IgG purified from the serum of anti–PD-1 therapy-treated aged mice (irAE Ig) were transferred into young or aged mice two times. Seven days after Ab infusion, the levels of indicated factors (*F*) and mouse IgG deposition in the lung (*G*) of host mice were monitored (n = 4–5). (*H* and *I*) B-cell depletion was performed in anti–PD-1 therapy-treated aged mice. H&E staining of the lung tissues (*H*) and the levels of indicated factors in the serum (*I*) are shown (n = 6–10). (Scale bars in *B*, *G*, and *H*: 100 or 200 μm.) Data are represented as mean ± SEM. One-way ANOVA with Turkey post hoc test was used; $*P < 0.05$, $**P < 0.01$, $***P < 0.001$.

aged, but not into young, mice (Fig. 2*F*). This implied that both aged mice-derived IgG and aged environment expressing Ab-reactive antigens were required for the organ toxicity, which was supported by IHC analysis with preferential accumulation of IgG in aged lung (Fig. 2*G*). To assess the contribution of B-cell response to irAE development, we depleted B cells from anti–PD-1 therapy-treated aged mice. As shown in Fig. 2*H*, B-cell depletion abolished the formation of TLS-like ectopic lymphocyte aggregates in lung. In accordance with this, the ICB-induced increases in tissue-damage–associated parameters, as well as IgG induction, were attenuated by B-cell depletion (Fig. 2*I*). These results suggest that B-cell activation and the subsequent auto-Ab production play a central role in irAE development.

IL-21–Producing CD4 T Cells Are Responsible for Anti–PD-1 Therapy-Induced irAEs. In line with previous findings that IL-21–producing T cells were preferentially induced in aged mice (24), aged lung-infiltrating CD4 T cells contained both interferon (IFN)-γ– and IL-21–producing cells, whereas CD8 T cells produced IFN-γ and less IL-21 (Fig. 3 *A* and *B*). IL-17-producing cells were also increased in aged mice (*SI Appendix*, Fig. S3*A*). Indeed, ICB treatment vigorously induced *Il21* expression in lung tissue, and its release was detected in bronchoalveolar lavage fluid (BALF) of tumor-bearing aged mice (Fig. 3 *C* and *D*). These were abrogated by CD4 T-cell depletion, suggesting that CD4 T cells functioned as a main source for IL-21 in aged irAE organs. Detailed analysis revealed that lung-infiltrating CD4 T cells in ICB-treated aged mice highly expressed Bcl-6, a master transcription factor of T follicular/peripheral helper (Tfh/Tph) cells (34), and the other Tfh marker, inducible T-cell costimulator, but not CXCR5 (*SI Appendix*, Fig. S3 *B* and *C*). These data imply $CXCR5^{-}$ Tph cells (29) are the main irAE organ-infiltrating cells. Similarly, an increase in $GL7^{+}CD95^{+}$ germinal center (GC)–phenotype

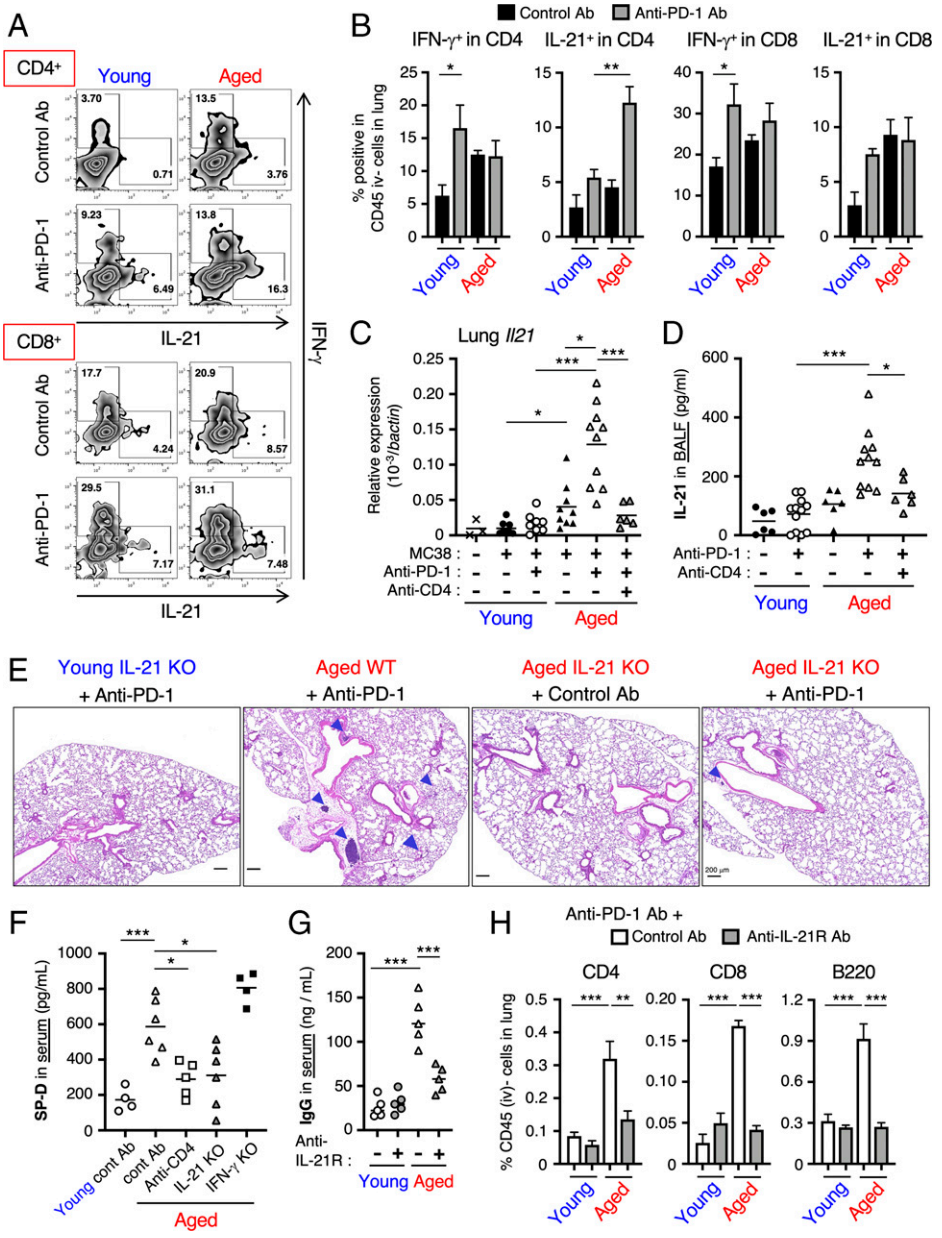

Fig. 3. IL-21 contributes to the age-related development of irAEs. (*A* and *B*) The representative dot plots (*A*) and the frequencies (*B*) of IL-21- and IFN-γ–producing cells in lung-infiltrating CD4 or CD8 T cells from MC38-bearing young or aged mice ($n = 4$). (*C* and *D*) *Il21* mRNA in whole lung tissues (*C*) and IL-21 levels in BALF (*D*) were assessed in young or aged mice with or without anti–PD-1 Ab administration ($n = 3$–10). (*E*) Representative H&E staining of lung sections. (Scale bars: 200 μm.) (*F*–*H*) Indicated mice were treated with anti–PD-1 Abs. The serum levels of SP-D (*F*) and IgG (*G*) and the frequencies of lung-infiltrating cell populations (*H*) were validated in tumor-bearing mice ($n = 4$–6). Data are represented as mean ± SEM. One-way ANOVA with Turkey post hoc test was used; $^{*}P < 0.05$, $^{**}P < 0.01$, $^{***}P < 0.001$.

B cells that promote Ab response was also observed in ICB-treated aged mice (*SI Appendix*, Fig. S3*D*).

Of note, while ICB-induced TLS organization and SP-D leakage were observed even in IFN-γ–deficient aged mice, those responses were attenuated by IL-21 deficiency (*SI Appendix*, Fig. S4, Fig. 3 *E* and *F*). Similar to IL-21–deficient aged mice, transient blockade of IL-21 activity with anti–IL-21 receptor (IL-21R) Ab in aged mice significantly attenuated the ICB-induced increase in hyperglobulinemia (Fig. 3*G*) and excessive infiltration of T and B cells in the lung (Fig. 3*H*). These findings indicate CD4 T-cell–derived IL-21, rather than IFN-γ, was responsible for ICB-induced irAE development.

IL-21 as a Potent Stimulator of CXCL13 Production. To better understand the molecular events underlying ICB-induced irAEs, we performed RNA sequencing (RNA-seq) and examined whole-gene transcripts of lung tissue altered by organism aging, ICB treatment, and IL-21 activity. All three components were considered responsible for irAE development. Principal-component analysis of each gene expression profile indicated the ICB-mediated change of lung environment (compared with control Ab-treated condition) was partially reversed by IL-21R blockade (*SI Appendix*, Fig. S5*A*). We detected substantial numbers of differentially expressed genes (DEGs): 868 genes in anti–PD-1 therapy-treated aged mice (compared with their younger counterparts), 311 genes (compared with control Ab-treated aged mice), and 294 genes (compared with aged mice with combined IL-21R blockade) (*SI Appendix*, Fig. S5*B*). A Venn diagram revealed that 44 genes were shared among the DEGs isolated from the aforementioned three comparison groups, and B-cell

homing chemokine (C-X-C motif) ligand 13 [CXCL13] gene (35) was isolated from the common DEGs (*SI Appendix*, Fig. S5*C*). This was confirmed by qPCR analysis (*SI Appendix*, Fig. S5*D*). Several Ig genes observed in the common DEGs support the idea that B-cell activation contributes to IL-21–mediated irAE symptoms, such as increased SP-D levels (*SI Appendix*, Fig. S5 *C* and *E*). Additionally, TLS hallmark gene signature including *Bcl6*, *Cxcl12*, *Cxcl13*, *Cxcr5*, and *Ccr7* (28, 29, 36) tended to be increased specifically in the lung of ICB-treated aged mice (*SI Appendix*, Fig. S5*F*), although *Ccl19*/*Ccl21* expression was below the detection threshold. Indeed, ICB-induced lymphocytic aggregates in aged lung contained peripheral node addressin-expressing high endothelial venules and $CD138^+$ plasma cells that characterize TLS (29), but $CD35^+$ follicular dendritic cells (FDCs) were not found (*SI Appendix*, Fig. S5*G*).

While substantial expression of CXCL13 was observed in aged lung even in the absence of tumor or ICB treatment, ICB dramatically upregulated CXCL13 expression (Fig. 4*A*), supporting the involvement of ICB-mediated T-cell activation in this event. In concordance with the generation of TLSs in irAE organs, a higher expression of CXCL13 was observed in kidney, lung, and liver, but not in colon, of aged mice (Fig. 4*B*). In contrast, CXCL13 expression in lymph nodes, spleen, and tumor tissues from ICB-receiving aged mice was significantly lower compared with those from their younger counterparts. IHC analysis revealed that CXCL13 was predominantly expressed within the TLS-like lymphoid follicles of aged lung, especially in macrophage marker $F4/80^+$ cells, but did not colocalize with $B220^+$ B cells (Fig. 4*C*), $CD3^+$ T cells, or α-smooth muscle $actin^+$ fibroblasts (*SI Appendix*, Fig. S6*A*). As in lung tissue, ICB-induced systemic (serum) and local (BALF) increase in CXCL13 were attenuated by CD4 T-cell depletion or IL-21 deficiency in tumor-bearing aged mice (Fig. 4 *D* and *E*). Based on these results including transcriptome analysis, we hypothesized that CXCL13 expression was directly regulated by IL-21 stimulation in irAE organs. To address this, we evaluated whether exogenous administration of IL-21 upregulated systemic levels of CXCL13 in vivo. As shown in Fig. 4*F*, administration of IL-21 induced CXCL13 in aged mice and, to a lesser extent, in young mice.

To confirm the *in vivo* results and to clarify the cellular source of CXCL13 in irAE organs, several cellular fractions were isolated from lung tissues. Consistent with the histological analysis of $CXCL13^+F4/80^+$ cells, $Ly6G^-CD11b^+$ monocyte/macrophage fraction from the lung of ICB-treated aged mice expressed higher levels of CXCL13 compared to their younger counterparts (*SI Appendix*, Fig. S6*B*), which was more prominent when exposed to IL-21 stimulation (Fig. 4*G* and *SI Appendix*, Fig. S6*C*).These results suggest that CD4 T-cell–derived IL-21 directly acts on myeloid cells in aged organs to potentiate their CXCL13 upregulation and ectopic mobilization of immune cells into irAE organs.

CXCL13 Is Essential for Ectopic Lymphoid Organogenesis and irAE Development. We next explored the contribution of CXCL13 to ICB-induced irAEs. Blocking CXCL13 activity with simultaneous administration of anti–PD-1 monoclonal Ab ameliorated the high levels of organ-toxicity–related serological indicators and serum Ig in aged mice (Fig. 5*A*). Supporting these findings, ICB-induced organization of TLS in liver, kidney, and lung was prevented by combined blockade of CXCL13 activity (Fig. 5*B*). Similar to IL-21R blockade, CXCL13 blockade in ICB-receiving aged mice significantly attenuated accumulation of B and T cells and IgG deposition in the lung (Fig. 5*C* and *SI*

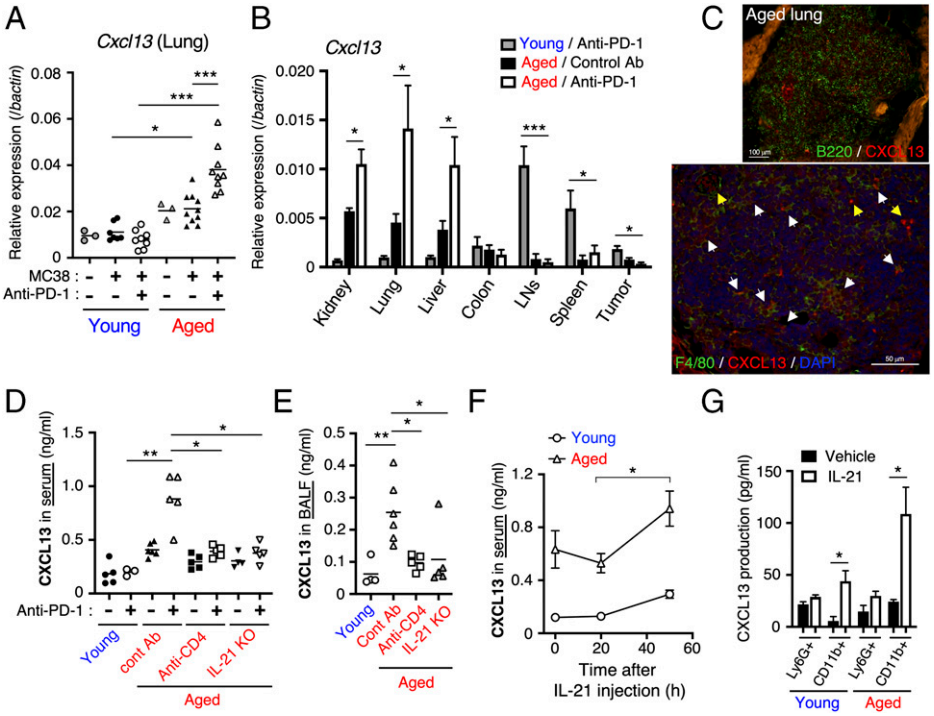

Fig. 4. Upregulation of CXCL13 is regulated by IL-21. MO4-bearing young or aged wild-type or IL-21–deficient mice were treated with anti–PD-1 Ab three times. (*A* and *B*) *Cxcl13* mRNA expression in the lung under various conditions (*A*; $n = 3$–10) or in various tissues from indicated mice (*B*; LNs, lymph nodes). (*C*) IHC staining with anti-CXCL13 (red) and anti-F4/80 or anti-B220 Abs (green) in the lung from young or aged mice with anti–PD-1 therapy. White and yellow arrows indicate $CXCL13^+$ cells with and without F4/80 staining, respectively. (Scale bars: 100 or 50 μm.) (*D* and *E*) The levels of CXCL13 in serum (*D*) and BALF (*E*) from indicated mice that were treated with anti–PD-1 Ab ($n = 4$–6). KO, knockout. (*F*) Recombinant IL-21 was injected into tumor-bearing mice, and the serum CXCL13 levels were assessed with time ($n = 5$). One-way ANOVA with Turkey post hoc test was used. (*G*) Indicated cell fractions isolated from lung tissues of tumor-bearing mice were stimulated with recombinant IL-21 in vitro, and CXCL13 production was assessed ($n = 3$). Two-tailed unpaired Student's *t* test was used. Data are represented as mean ± SEM; $^*P < 0.05$, $^{**}P < 0.01$, $^{***}P < 0.001$.

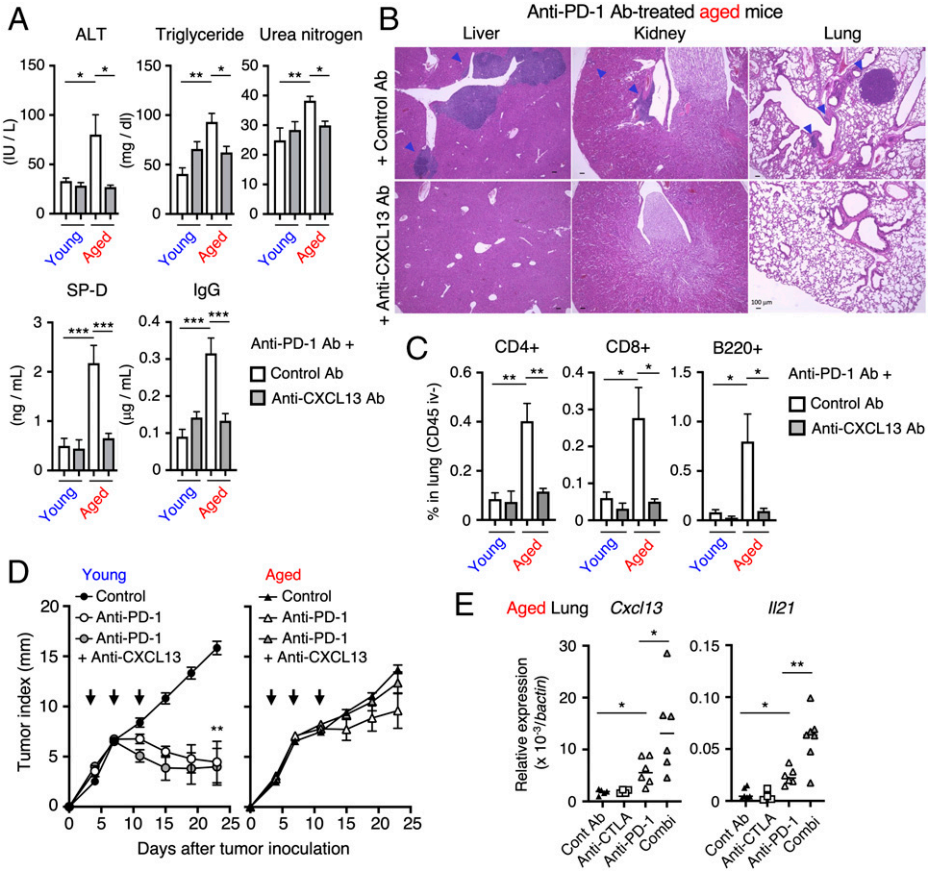

Fig. 5. Age-associated increase in CXCL13 promotes irAE development. MC38-bearing young or aged mice were treated three times with anti–PD-1 therapy together with CXCL13 blockade. Four days after the third treatment, the levels of indicated factors in blood (*A*; $n = 4$–6), the histological tissue sections of indicated tissues (*B*, H&E staining), and the frequencies of indicated populations in the lung (*C*; $n = 4$–5) were assessed. (Scale bars in *B*: 100 μm.) Outgrowth of MC38 was measured with time ($n = 6$). Arrows indicate the timing of Abs administrations (*D*). (*E*) MC38-bearing aged mice were treated three times with monotherapy or combination therapy with anti–PD-1 and anti–CTLA-4 Abs. mRNA expression of *Cxcl13* and *Il21* in the lung were determined ($n = 5$–6). Data are shown as mean ± SEM. One-way ANOVA with Turkey post hoc test was used; $^*P < 0.05$, $^{**}P < 0.01$, $^{***}P < 0.001$.

Appendix, Fig. S6*D*). In contrast to irAE development, antitumor activity of ICB was not diminished by CXCL13 blockade in MC38-bearing young mice. In aged mice, tumor burden persisted even with a combined blockade of CXCL13, as observed in mice solely administered with anti–PD-1 monoclonal Ab. (Fig. 5*D*). Confirming the effect of CXCL13 on irAE symptoms, the anti–PD-1 therapy-induced expression of *Cxcl13* and *Il21* was significantly augmented by additional CTLA-4 blockade in aged mice (Fig. 5*E*), which coincided with exacerbation of irAEs in this regimen (*SI Appendix*, Fig. S2*B*). These results suggest that CXCL13 is indispensable for the aberrant TLS generation and subsequent irAE development, while providing inconsequential effects on antitumor activity of ICBs.

Considering the use of corticosteroids as a primary strategy to manage irAE symptoms in clinical settings, we assessed the effect of steroids on ICB-mediated CXCL13 upregulation and subsequent TLS generation. Treatment with steroid in ICB-receiving aged mice significantly inhibited the ectopic accumulation of T and B cells (*SI Appendix*, Fig. S6*E*). Concomitant with reduced ectopic immune response in the lung, systemic CXCL13 induction was also alleviated, resulting in reduced Ab response (*SI Appendix*, Fig. S6*F*). This implied that immunosuppressive activity of corticosteroids on irAE symptoms might be partially attributed to its detrimental effect on CXCL13 production.

Association of Systemic CXCL13 Levels with irAE in Cancer Patients. Given that systemic upregulation of CXCL13 was associated with increased risk of irAEs in the mouse model, we evaluated levels of CXCL13 in plasma from NSCLC patients before and 2 or 3 wk after initiation of anti–PD-(L)1 therapy. This timing was chosen to be before the median timing of irAE onset (37). Patient and healthy donor information is described in *SI Appendix*, Tables S1 and S2. There was no significant difference in plasma levels of CXCL13 between healthy donors and patients before treatment. Their CXCL13 levels increased by ∼1.5-fold after ICB treatment (Fig. 6*A*, *Top*). Interestingly, the levels of CXCL13 were significantly higher in the patients with irAEs compared to those without irAEs (Fig. 6*A*, *Bottom*). The increase in CXCL13 during the treatment was remarkable in irAE patients (Fig. 6*B*). Univariate logistic analysis demonstrated the levels of CXCL13 were significantly associated with the development of irAEs (odds ratio = 19.31, 95% CIs; lower 2.32, upper 160.49; $P = 0.006$) (*SI Appendix*, Table S3). We found that the expression levels of *Il21* in peripheral CD4 T cells from the irAE patients were significantly higher than those from the patients without irAEs (*SI Appendix*, Fig. S7*A* and Table S3) and exhibited a proportional increase along with an increase in the plasma level of CXCL13, while no statistically significant association between *ifng* expression and CXCL13 levels was observed (Fig. 6*C* and *SI Appendix*, Table S3). Although the ages of patients with NSCLC tended to correlate with CXCL13 levels ($P = 0.08$), we did not find statistically significant correlation of the age with any clinical parameters except PD-L1 expression in cancerous tissues (*SI Appendix*, Table S4). In contrast to those factors, the levels of C-reactive protein (CRP) and IL-6, clinical blood parameters for inflammatory

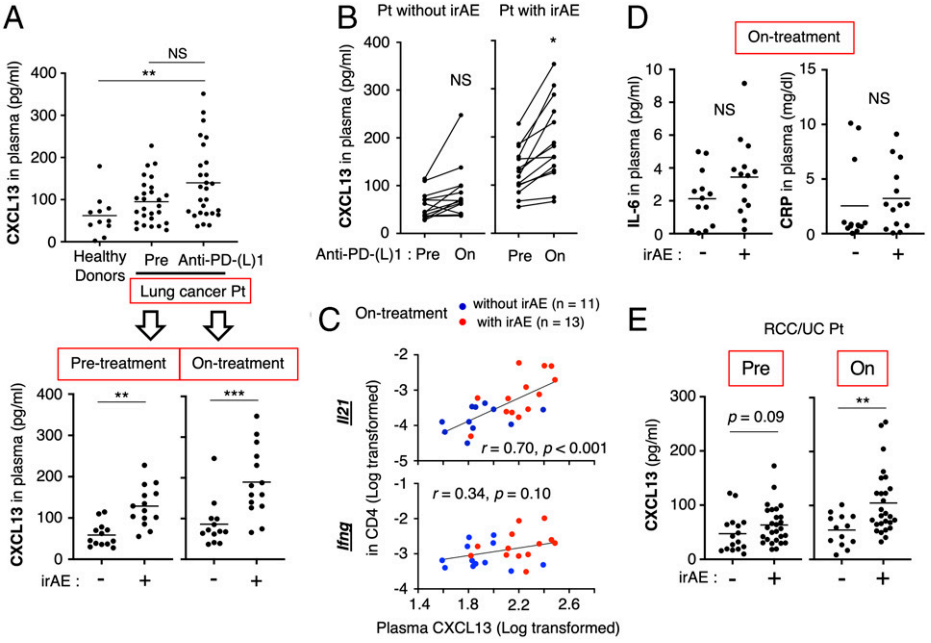

Fig. 6. The levels of CXCL13 are associated with the incidence of anti–PD-1 therapy-induced irAEs. (*A*) (*Top*) Levels of CXCL13 were analyzed in plasma from NSCLC patients (n = 27) or healthy donors (n = 11). One-way ANOVA with Turkey post hoc test was used; $^{**}P < 0.01$. (*Bottom*) CXCL13 levels were further analyzed before (Pretreatment) and 2 wk after initial ICB treatment (On-treatment) in the patients with (n = 14) or without (n = 13) irAEs. (*B*) Changes in CXCL13 level were also assessed. (*C*) The levels of (*Left*) IL-6 and (*Right*) CRP were measured at On-treatment in the NSCLC patients with or without irAEs. (*D*) Correlation between plasma levels of CXCL13 and mRNA expression levels of (*Top*) *Il21* or (*Bottom*) *Ifng* in CD4 T cells of NSCLC patients (On-treatment) were examined by linear regression analyses. The data were plotted as natural logarithm transformed values. (*E*) The levels of CXCL13 before (Pre) and 2 wk after initial treatment with ICB (On) in RCC/UC patients with (n = 14) or without (n = 27) irAEs. Nonparametric Mann–Whitney U test was used; $^{*}P < 0.05$, $^{**}P < 0.01$, $^{***}P < 0.001$. Pt, patients; NS, not significant.

responses, were not associated with irAE incidence (Fig. 6*D* and *SI Appendix*, Table S3), suggesting that the increase in CXCL13 is not the consequence of systemic inflammatory response.

To evaluate the validity of this finding across other cancer types, we assessed the plasma levels of CXCL13 in patients with renal cell carcinoma (RCC)/urothelial cancer (UC). Similar to NSCLC patients, we found a significant increase in CXCL13, but not CRP, in RCC/UC patients with irAEs, especially during treatment, as compared with the patients without irAEs (Fig. 6*E*, *SI Appendix*, Fig. S7 *B–D*, and Table S5). These results suggest that higher levels of CXCL13 are associated with increased risk for irAE incidence, regardless of tumor types. We did not find an obvious correlation between CXCL13 levels and the grade of irAEs (*SI Appendix*, Fig. S7*E*).

Consistent with recent reports showing a higher clinical benefit in patients who experienced ICB-related irAEs than in those who did not (20, 37), patients with irAEs tended to have longer progression-free survival (PFS) than the patients without irAEs in NSCLC (*SI Appendix*, Fig. S7*F*). However, RCC/UC patients did not exhibit a similar association between toxicity and response rate (*SI Appendix*, Fig. S7*G*). On the other hand, there was no significant difference in the duration of PFS when stratified according to CXCL13 levels during ICB treatment (*SI Appendix*, Fig. S7 *H* and *I*). Altogether, our data imply that elevated levels of CXCL13 have an independent predictive role in irAE development, irrespective of therapeutic responsiveness in cancer patients.

Discussion

Because cancer prevalence is higher in elderly individuals, the influence of organism aging on ICB-mediated immune responses should be given serious consideration. The age-associated immunological changes, "immunosenescence," have been reported to impact the responsiveness to cancer immunotherapies (24, 25, 38) and could also have meaningful implications for ICB-induced autoimmune-like toxicity in cancer patients (19–21). In this study, we did not observe obvious toxicity in young mice. However, aged animals developed anti–PD-1 therapy-induced irAE symptoms. Our data suggest that organism aging accelerates the breakdown of self-tolerance maintained by PD-1/PD-L1 interaction. This result resonates with the fact that deficiency of PD-1/PD-L1 interaction can potentially activate the production of auto-Abs, resulting in autoimmune-disease–like symptoms, especially in advanced age (4). Here, utilizing this experimental model for ICB-induced irAEs, we found 1) Tph-like CD4 T cells potentiated auto-Ab production in response to ICB through IL-21 production; 2) IL-21 acted as a direct stimulator for CXCL13 production and subsequent TLS organization in irAE organs; and 3) systemic increases in CXCL13 are associated with irAE occurrence (Graphical schema; *SI Appendix*, Fig. S7*J*). Our preclinical findings with cancer patients, indeed, proved the predictive relevance of CXCL13 and IL-21 for irAE development.

A systemic increase in CXCL13 in irAE patients supported a mechanistic similarity between irAEs and autoimmune diseases because CXCL13 serves as a biomarker of autoimmune diseases such as rheumatoid arthritis, systemic lupus erythematosus, and Sjogren's syndrome, and its systemic levels were correlated with their pathologic deterioration (39). Whereas increased levels of CXCL13 can be monitored immediately after ICB treatment in aged mice and cancer patients, a systemic increase of Ig, the classical biomarker for autoimmune diseases, was measurable only after multiple rounds of ICB administration in our model. Considering local pathogenicity, cognate T-B interaction and subsequent autoreactive Ab production are likely to be primed in irAE organs. However, direct assessment of reactive GC B cells and Tfh/Tph-like CD4 T cells in noncancerous organs is rarely available from cancer patients. Therefore, by monitoring CXCL13 in plasma as a promising biomarker reflective of the

GC response, risk of irAEs may be predictable before its incidence because the median timing of irAE onset is 8.4 wk after initial treatment (37). Furthermore, it is expected that combined monitoring of auto-Abs specific for irAE-associated self-antigens, rather than total IgG, would be more appropriate for diagnosis of certain type(s) of irAEs.

Our preclinical model representing auto-Ab–mediated organ toxicities was consistent with higher levels of auto-Abs in patients with irAEs such as pneumonitis, thyroiditis, and hypophysitis (5, 12) but did not recapitulate symptoms of diarrhea/colitis observed in irAE patients. Similar to autoimmune diseases, irAE symptoms are estimated to be divided into several types of organ-specific toxicities depending on the characteristics of auto-antigens, T cells, or B-cell-mediated immune response (11–16). Indeed, the monotherapy with anti–CTLA-4 Abs did not induce obvious irAE-related events such as increased tissue-infiltrating cells, Ab response, and organ damages in our aged mouse model. This implies that the autoimmune-prone phenotype of aged mice, such as aberrant immune and inflammatory responses, is likely to mimic only certain disease types in irAEs, with wide ranging toxicity profiles (5) and autoimmune diseases (40).

The indistinct association between patients' ages and irAE-associated factors in the cohort with a limited number of patients might be caused by the genetically diverse backgrounds and differential exposures of environmental factors experienced by individual patients, which might lead to the difference in their senescent statuses and immune responses, including the responsiveness to the immunotherapy among the heterogeneous individuals even at the same age. On the other hand, a recent study with a large number of lung cancer patients reported that elderly patients exhibited a higher incidence of pulmonary toxicity from anti–PD-(L)1 therapy (21). This report supports our hypothesis that age-related immunological change(s) have an impact on irAE development. For earlier in-trial decision-making and heightened management of irAEs, it is necessary to further investigate what kinds of diseases and immunotherapeutic regimens the IL-21-CXCL13-auto-Ab axis is largely at play in and whether this axis and a patient's age stratify particular types and grades of irAEs by utilizing larger cohorts across several tumor types.

CXCL13 is the ligand for CXCR5 expressed on B cells and Tfh, and it is responsible for their migration to B-cell follicles and plays a role in GC formation (29, 35). This is partially consistent with our findings that blockade of CXCL13 or IL-21 significantly diminished ICB-mediated accumulation of both T and B cells in irAE organs and TLS formation. However, CXCR5 expression was detected only on B cells, not on T cells, residing in irAE organs. A regulatory mechanism for T-cell accumulation within irAE organs remains unclear. One possible explanation is that T cells are mobilized to irAE organs through chemokine receptors other than CXCR5. In addition, defective B-cell recruitment into irAE organs due to reduced CXCL13 activity might secondarily abrogate B-cell-mediated antigen presentation for clonal expansion of Tfh/Tph (41), resulting in decreased local division of T cells and TLS maturation. Furthermore, this cognate T-B interplay is likely to be promoted by IL-21–producing CD4 T cells because IL-21 contributes to the maintenance of both cell populations through retaining their Bcl6 expression (42). Aside from the T-B interplay, we proposed here that IL-21 functioned as a direct inducer of CXCL13 production from $CD11b^+$ myeloid cell component in aged mice (*SI Appendix*, Fig. S7*J*). Collectively, it is postulated that local Ab response and irAE symptoms were exacerbated by the dual function of IL-21: the feed-forward mechanism between T and B cells and direct CXCL13 induction within the TLS. Remarkably, the difference in CXCL13 production from aged versus young lung-derived cells, even in vitro, suggests the age-associated change in cellular constituents or intrinsic ability to produce CXCL13. Although several cell populations—including Tfh, monocytes/macrophages, and $CD35^+$ FDCs—have been reported to produce CXCL13 under different settings (29, 35), detailed analysis of CXCL13-producing subset(s) in our irAE model will provide a fundamental insight into organism aging or cellular senescence.

The present study provided a rationale for targeting the IL-21/CXCL13-auto-Ab axis in circumventing anti–PD-1 therapy-induced irAEs. We have demonstrated that transient CXCL13 blockade for irAE management during the initial phase of ICB does not interfere with durable therapeutic effect in young mice, although long-lasting inactivation or complete deficiency of CXCL13 may result in insufficient immunosurveillance (43). On the other hand, higher systemic levels of CXCL13 during ICB treatment were not accompanied by better therapeutic efficacy in aged mice and cancer patients. These results were seemingly discrepant with recent studies suggesting a predictive value of higher CXCL13 expression and TLS organization in tumor tissues for improved therapeutic benefit of ICB in the patients (36, 43). The most reasonable cause for the lower therapeutic efficacy of ICB in aged mice, albeit the vigorous CXCL13 upregulation, is age-associated fundamental dysfunction in T-cell–mediated responses, such as functional defects of antitumor effector CD8 T cells and Th1 cells, and reduced T cell receptor repertories (24, 25, 44). Given this premise, it is highly possible that in aged animals, ICB does not provide substantial therapeutic benefits even if CXCL13-mediated TLS formation would be efficiently induced upon ICB. In addition to this possibility, the discordant antitumor immunity with TLS formation in irAE organs in aged mice can be explained by distinct regulatory mechanisms underlying CXCL13-mediated TLS organization and differential cellular sources of CXCL13 between tumor tissues and irAE organs. Indeed, in contrast to the irAE organs, CXCL13 expression in tumor tissues of aged mice was significantly lower than in young mice. Furthermore, CXCL13 was expressed in myeloid cells but not αSMA^+ fibroblasts in irAE organs, while cancer-associated (myo)fibroblasts have been reported to produce CXCL13 to promote TLS formation in tumor tissues (45, 46).

Theoretically, approaches to reduce the risk of irAEs without compromising antitumor effects are feasible if irAE-eliciting immune responses and antitumor immunity are regulated by distinct mechanisms. This idea was supported by our findings that the irAE-associated immune reactions were induced even with IFN-γ deficiency, one of the most critical cytokines in antitumor activity (22, 38). This also coincided with the higher expression of *Il21* rather than *Ifng* in CD4 T cells from irAE patients. From these perspectives that irAEs are not necessarily concurrent with antitumor immunity, it is conceivable that augmentation of antitumor immune response is compatible with irAE management. In order to balance both interventions, target(s) specifically distinguishing the immune response in tumor tissues from irAE-associated TLS formation need to be clarified. In addition to CXCL13, CCL19 and CCL21 could be considered as candidates for this purpose because TLS formation and expression of *Ccl19* and *Ccl21* in tumor tissues were closely accompanied by higher therapeutic efficacy of ICB (36). Similar to the situation in ICB responders, CCL19 and CCL21 also play a critical role in TLS organization during viral elimination, irrespective of CXCL13 activity (28). Conversely, our RNA-seq analysis demonstrated *Ccl19* and *Ccl21* expression was hardly detected in irAE organs,

implying a distinct dependency of these chemokines on TLS generation in tumor site from that in irAE organs. Considering these phenomena, CCL19 and CCL21 may serve as factors for potentiating the TLS generation in tumor sites and subsequent antitumor activity, but not for priming irAE development. Our findings support the fact that activation of B cells, a downstream target of CXCL13, is also correlated with the occurrence and onset of irAEs (13). However, modification of B-cell response as a treatment for irAEs may be a concern because TLS-related B cells are beneficial in cancer immunosurveillance (36). In addition to the demand in elucidating how and when these factors contribute to irAE development, detailed analysis about the immunological dilemma between antitumor response and irAE development will be advisable.

Materials and Methods

Mice. All experimental mice–including inbred C57BL/6J, IL-6–deficient, IL-21–deficient, and IFN-γ–deficient mice–were housed at the Center for Animal Resources and Development, Kumamoto University and Kyoto University (see *SI Appendix, Materials and Methods* for more details). All procedures were approved by the Institutional Animal Committee of Kumamoto University and Kyoto University and performed in accordance with accepted guidelines.

Tumor Inoculation and Treatment. OVA-expressing melanoma MO4 (47) was kindly provided by Kenneth L. Rock (UMass Medical School). Colon carcinoma MC38 and CT26 were provided by Kerafast and RIKEN BRC Cell Bank, respectively. Mice were inoculated subcutaneously with 1×10^5 CT26, MO4, or 4×10^5 MC38. Tumor growth was monitored by measuring every 3 or 4 d with calipers using the two largest perpendicular axes until the volume (length × width) of the tumor exceeded 2,000 mm^2, and the size was expressed as tumor index, which is the square root of length × width, as previously described (22). The Abs administrated in mice were described in *SI Appendix, Materials and Methods*.

Patients. Patients with locally advanced and metastatic NSCLC who were treated with anti–PD-1 or anti–PD-L1 Ab and patients with RCC/UC treated with anti–PD-1 Ab or combination of anti–PD-1/CTLA-4 Ab, and for whom pre- and on-treatment (2 or 3 wk post-initial administration) plasma samples were available, were identified at Kumamoto University Hospital (NSCLC; $n = 27$, RCC/UC; $n = 17$) and Toranomon Hospital (RCC/UC; $n = 29$). Plasma and peripheral blood mononuclear cells from Ficoll-separated blood were cryopreserved until experimental use. Samples in this study were collected from May 2018 to January 2021 and were utilized in accordance with the Declaration of Helsinki. All the study protocols were approval by the Institutional Review Boards of Kumamoto University (protocols 2036 and 1864) and Toranomon Hospital (protocol 1690). Informed consent was obtained from all the subjects, including healthy donors. The information regarding patients and healthy donors is described in *SI Appendix*, Tables S1 and S2, respectively. PFS was defined as the time from the start of ICB treatment until disease progression, determined by imaging and/or clinical observation according to the treating oncologist's clinical judgment, and was assessed until March 2021 in the patients for whom sequential blood samples were available. Responses were scored according to Response Evaluation Criteria in Solid Tumors (RECIST) 1.1 criteria. Their development of irAEs (based on standard laboratory values and clinical examinations) were followed up 6 mo post-initial treatment using Common Terminology Criteria for Adverse Events version 5.0. The levels of CRP and treatment outcomes were extracted from patient records.

Flow Cytometric Analysis. For removal of blood-circulating immune cells from the analysis, APC-Cy7–labeled anti-CD45 Abs (Biolegend, 3 μg/mouse) were intravenously injected into the mice prior to euthanasia. Tissues including tumors were minced with razors and analyzed for messenger RNA (mRNA) expression or digested with 2.5 mg/mL collagenase D (Roche) and 0.1 mg/mL DNase I (Sigma) for 30 min. Cell suspensions were stained with the Abs described in *SI Appendix, Materials and Methods*. Immunofluorescence images and the data were analyzed using FACSVerse or Fortessa (BD Biosciences) and FlowJo software (Tree Star), respectively.

Measurements of Lung Function. Mice were anesthetized using pentobarbital sodium (40 mg/kg, Somnopentyl, Kyoritsu) and xylazine (2.0 mg/kg, Seractal, Bayer) via intraperitoneal injection and then were tracheostomized and connected to a computer-controlled small animal ventilator (flexiVent, SCIREQ). Pulmonary functional parameters were measured with mechanical ventilation set at 150 breaths/min with a tidal volume of 10 mL/kg on 100% inspired oxygen and at a positive end-expiratory pressure of 3 cm H_2O. For each parameter, a coefficient of determination of 0.95 was the lower limit for accepting a measurement. Animals were closely monitored for lung collapse and expansion.

For estimation of wet-to-dry ratios as an index of pulmonary edema and congestion (33), mice were euthanized, and the lower portions of the left lung were immediately weighed. After drying at 56 °C for 18 h, each lung was weighed again to calculate the wet-to-dry lung weight ratio.

BALF Preparation. The lung was lavaged two times with 0.75 mL ice-cold phosphate-buffered saline (PBS). PBS was instilled into the lung and allowed to equilibrate for 30 s before recovery. The two aliquots were pooled and centrifuged at 900 × *g* for 5 min at 4 °C, and the supernatants were stored at −80 °C until further analysis.

Measurement of Cytokines, Serologic Clinical Markers, and Ig. Serum was harvested 15 d after tumor inoculation. The concentrations of murine IL-21, SP-D, murine and human CXCL13, or IL-6 were quantified by enzyme-linked immunosorbent assay (ELISA) (R&D Systems). For total IgG quantification, the Sigma ELISA kit was utilized. The other serum components were quantified by high-throughput chemical analyzer JCA-BM6050 (Japan Electron Optics Laboratories) according to the manufacturer's protocols.

Purification of Ig Mouse Serum. Mouse Ig was purified from pooled serum using protein-G column (GE Healthcare). The eluted Igs were concentrated using a Centricon-30 (Amicon). Then, 250 μg purified Ig was intravenously injected two or three times every 5 d.

RNA Extraction, cDNA Synthesis, Real-Time PCR, and RNA-Seq. Total RNA was extracted using TRIzol reagent (Thermo Fisher Scientific) and then purified using RNeasy Plus Mini Kit (QIAGEN). Complementary DNA (cDNA) was synthesized by reverse transcription with ReverTra Ace (TOYOBO). Real-time qPCR was performed on a ViiA7 or one-step real-time PCR System using Taqman Universal PCR Master Mix reagents (Applied Biosystems) and probes described in *SI Appendix, Materials and Methods*. Expression levels for each gene were normalized to expression of *Gapdh* or *bactin* using the comparative 2[−ΔΔCT] method.

RNA deep sequencing was conducted on total RNAs extracted from whole-lung tissues of each mouse group, as described in *SI Appendix, Materials and Methods*. The data have been deposited in the Gene Expression Omnibus (accession number GSE184000).

Histological Evaluation and IHC. Murine tissues were fixed with 4% (wt/vol) paraformaldehyde and routinely embedded in paraffin wax, sectioned, and stained with hematoxylin and eosin (H&E). For IHC of paraffine sections, slices were deparaffinized and treated with 0.3% H_2O_2. Following antigen retrieval with pressure cooker (DAKO) or microwave, the slices were stained with the Abs described in *SI Appendix, Materials and Methods*. Integrated intensity and proportion of positive cells rounded of interest in immunofluorescence images were semiquantitatively analyzed using ImageJ (NIH).

Isolation of Primary Immune Cells from Lung Tissue. For isolation of primary immune cells from mouse lung tissue or from peripheral blood mononuclear cells of the patients with NSCLC, appropriate microbeads (Miltenyi Biotec) were utilized. The details were described in *SI Appendix, Materials and Methods*.

Statistical Analysis. Multiple group comparisons were performed by one-way ANOVA followed by Tukey–Kramer post hoc test using GraphPad Prism 7.0 software. In some experiments, differences were determined by two-tailed Student's *t* test, assuming unequal variance, or by Mann–Whitney *U* test. The detailed methods for analyses of multivariables from patients' samples are described in *SI Appendix, Materials and Methods*. The level of statistical significance was set at $P < 0.05$.

Data Availability. RNA deep sequencing data have been deposited in the Gene Expression Omnibus (accession number GSE184000) (48). All other study data are included in the article and/or *SI Appendix*.

ACKNOWLEDGMENTS. We thank Drs. T. Honjo, K. Murakami, K. Chamoto, T. Yaguchi, M. Tajima, Mr./Ms. M. Kataoka, K. Iguchi, and M. Shikata at Center for Cancer Immunotherapy and Immunobiology of Kyoto University and all lab members at Department of Immunology of Kumamoto University for helpful discussions and technical support. This work was supported by JSPS KAKENHI No. 21H02788 to H.T. and Yanai Fund. H.T. was also supported by The Shin-Nihon Foundation of Advanced Medical Research and The Princess Takamatsu Cancer Research Fund.

Author affiliations: [a]Division of Clinical Immunology and Cancer Immunotherapy, Center for Cancer Immunotherapy and Immunobiology, Graduate School of Medicine, Kyoto University, Kyoto, Japan; [b]Department of Immunology, Graduate School of Medical Sciences, Faculty of Life Sciences, Kumamoto University, Kumamoto, Japan; [c]Department of Cell Pathology, Graduate School of Medical Sciences, Faculty of Life Sciences, Kumamoto University, Kumamoto, Japan; [d]Department of Respiratory Medicine, Graduate School of Medical Sciences, Faculty of Life Sciences, Kumamoto University, Kumamoto, Japan; [e]Department of Medical Oncology, Toranomon Hospital, Tokyo, Japan; [f]Department of Urology, Graduate School of Medical Sciences, Faculty of Life Sciences, Kumamoto University, Kumamoto, Japan; and [g]Laboratory of Clinical Pharmacology and Therapeutics, Faculty of Pharmaceutical Sciences, Sojo University; Kumamoto, Japan

Author contributions: H.T., Y.K., and H.O. designed research; H.T., Y.K., Y.T., Y.M., T.M., K.I., T. Kimura, T.I., Y.F., H.Y., T. Kamba, and T.S. performed research; H.T., Y.K., Y.T., Y.M., T.M., T.I., and H.O. analyzed data; and H.T., Y.K., Y.T., and H.O. wrote the paper.

Competing interest statement: Y.M. reports receiving personal fees from Ono Pharmaceutical, Bristol Myers Squibb, MSD, and Takeda and attended as Advisory Board personal member of Chugai Pharmaceutical Co. and Takeda; Local PI and Institutional Financial interest from MSD and Ono Pharmaceutical. T. Kamba reports receiving personal fees and nonfinancial supports from Ono Pharmaceutical. All of them are outside this submitted work. The remaining authors have no competing interests to declare.

1. M. Reck *et al.*; KEYNOTE-024 Investigators, Pembrolizumab versus chemotherapy for PD-L1-positive non-small-cell lung cancer. *N. Engl. J. Med.* **375**, 1823–1833 (2016).
2. J. Larkin *et al.*, Combined Nivolumab and Ipilimumab or monotherapy in untreated melanoma. *N. Engl. J. Med.* **373**, 23–34 (2015).
3. J. D. Wolchok *et al.*, Overall survival with combined Nivolumab and Ipilimumab in advanced melanoma. *N. Engl. J. Med.* **377**, 1345–1356 (2017).
4. T. Okazaki *et al.*, Autoantibodies against cardiac troponin I are responsible for dilated cardiomyopathy in PD-1-deficient mice. *Nat. Med.* **9**, 1477–1483 (2003).
5. W. Hu, G. Wang, Y. Wang, M. J. Riese, M. You, Uncoupling therapeutic efficacy from immune-related adverse events in immune checkpoint blockade. *iScience* **23**, 101580 (2020).
6. E. De Martin, J. M. Michot, O. Rosmorduc, C. Guettier, D. Samuel, Liver toxicity as a limiting factor to the increasing use of immune checkpoint inhibitors. *JHEP Rep* **2**, 100170 (2020).
7. F. C. Santini *et al.*, Safety and efficacy of re-treating with immunotherapy after immune-related adverse events in patients with NSCLC. *Cancer Immunol. Res.* **6**, 1093–1099 (2018).
8. K. Esfahani *et al.*, Moving towards personalized treatments of immune-related adverse events. *Nat. Rev. Clin. Oncol.* **17**, 504–515 (2020).
9. A. Tokunaga *et al.*, Selective inhibition of low-affinity memory $CD8^+$ T cells by corticosteroids. *J. Exp. Med.* **216**, 2701–2713 (2019).
10. X. Bai *et al.*, Early use of high-dose glucocorticoid for the management of irAE is associated with poorer survival in patients with advanced melanoma treated with anti-PD-1 monotherapy. *Clin. Cancer Res.* **27**, 5993–6000 (2021).
11. F. Berner *et al.*, Association of checkpoint inhibitor-induced toxic effects with shared cancer and tissue antigens in non-small cell lung cancer. *JAMA Oncol.* **5**, 1043–1047 (2019).
12. S. A. Tahir *et al.*, Autoimmune antibodies correlate with immune checkpoint therapy-induced toxicities. *Proc. Natl. Acad. Sci. U.S.A.* **116**, 22246–22251 (2019).
13. R. Das *et al.*, Early B cell changes predict autoimmunity following combination immune checkpoint blockade. *J. Clin. Invest.* **128**, 715–720 (2018).
14. C. Calabrese *et al.*, Polymyalgia rheumatica-like syndrome from checkpoint inhibitor therapy: Case series and systematic review of the literature. *RMD Open* **5**, e000906 (2019).
15. E. P. Hoefsmit, E. A. Rozeman, J. B. A. G. Haanen, C. U. Blank, Susceptible loci associated with autoimmune disease as potential biomarkers for checkpoint inhibitor-induced immune-related adverse events. *ESMO Open* **4**, e000472 (2019).
16. C. S. Pai *et al.*, Tumor-conditional anti-CTLA4 uncouples antitumor efficacy from immunotherapy-related toxicity. *J. Clin. Invest.* **129**, 349–363 (2019).
17. B. D. Smith, G. L. Smith, A. Hurria, G. N. Hortobagyi, T. A. Buchholz, Future of cancer incidence in the United States: Burdens upon an aging, changing nation. *J. Clin. Oncol.* **27**, 2758–2765 (2009).
18. C. Parry, E. E. Kent, A. B. Mariotto, C. M. Alfano, J. H. Rowland, Cancer survivors: A booming population. *Cancer Epidemiol. Biomarkers Prev.* **20**, 1996–2005 (2011).
19. A. S. Betof *et al.*, Impact of age on outcomes with immunotherapy for patients with melanoma. *Oncologist* **22**, 963–971 (2017).
20. H. Matsuoka *et al.*, Correlation between immune-related adverse events and prognosis in patients with various cancers treated with anti PD-1 antibody. *BMC Cancer* **20**, 656 (2020).
21. X. Huang *et al.*, Age-associated changes in adverse events arising from anti-PD-(L)1 therapy. *Front. Oncol.* **11**, 619385 (2021).
22. H. Tsukamoto *et al.*, Combined blockade of IL6 and PD-1/PD-L1 signaling abrogates mutual regulation of their immunosuppressive effects in the tumor microenvironment. *Cancer Res.* **78**, 5011–5022 (2018).
23. J. Manola, M. Atkins, J. Ibrahim, J. Kirkwood, Prognostic factors in metastatic melanoma: A pooled analysis of Eastern Cooperative Oncology Group trials. *J. Clin. Oncol.* **18**, 3782–3793 (2000).
24. H. Tsukamoto, S. Senju, K. Matsumura, S. L. Swain, Y. Nishimura, IL-6-mediated environmental conditioning of defective Th1 differentiation dampens antitumour immune responses in old age. *Nat. Commun.* **6**, 6702 (2015).
25. Y. Nakajima, K. Chamoto, T. Oura, T. Honjo, Critical role of the $CD44^{low}CD62L^{low}$ $CD8^+$ T cell subset in restoring antitumor immunity in aged mice. *Proc. Natl. Acad. Sci. U.S.A.* **118**, e2103730118 (2021).
26. C. Winkler *et al.*, Comprehensive characterisation of pulmonary and serum surfactant protein D in COPD. *Respir. Res.* **12**, 29 (2011).
27. F. Moazed *et al.*, Cigarette smokers have exaggerated alveolar barrier disruption in response to lipopolysaccharide inhalation. *Thorax* **71**, 1130–1136 (2016).
28. J. Rangel-Moreno, J. E. Moyron-Quiroz, L. Hartson, K. Kusser, T. D. Randall, Pulmonary expression of CXC chemokine ligand 13, CC chemokine ligand 19, and CC chemokine ligand 21 is essential for local immunity to influenza. *Proc. Natl. Acad. Sci. U.S.A.* **104**, 10577–10582 (2007).
29. A. Nerviani, C. Pitzalis, Role of chemokines in ectopic lymphoid structures formation in autoimmunity and cancer. *J. Leukoc. Biol.* **104**, 333–341 (2018).
30. E. H. Choy *et al.*, Translating IL-6 biology into effective treatments. *Nat. Rev. Rheumatol.* **16**, 335–345 (2020).
31. T. T. Hansel, H. Kropshofer, T. Singer, J. A. Mitchell, A. J. George, The safety and side effects of monoclonal antibodies. *Nat. Rev. Drug Discov.* **9**, 325–338 (2010).
32. J. J. Pillow, T. R. Korfhagen, M. Ikegami, P. D. Sly, Overexpression of TGF-alpha increases lung tissue hysteresivity in transgenic mice. *J. Appl. Physiol.* **91**, 2730–2734 (2001).
33. H. Dai *et al.*, Mechanical ventilation modulates Toll-like receptors 2, 4, and 9 on alveolar macrophages in a ventilator-induced lung injury model. *J. Thorac. Dis.* **7**, 616–624 (2015).
34. K. Hatzi *et al.*, BCL6 orchestrates Tfh cell differentiation via multiple distinct mechanisms. *J. Exp. Med.* **212**, 539–553 (2015).
35. K. M. Ansel *et al.*, A chemokine-driven positive feedback loop organizes lymphoid follicles. *Nature* **406**, 309–314 (2000).
36. R. Cabrita *et al.*, Tertiary lymphoid structures improve immunotherapy and survival in melanoma. *Nature* **577**, 561–565 (2020).
37. M. Sznol *et al.*, Pooled analysis safety profile of Nivolumab and Ipilimumab combination therapy in patients with advanced melanoma. *J. Clin. Oncol.* **35**, 3815–3822 (2017).
38. V. Hurez *et al.*, Mitigating age-related immune dysfunction heightens the efficacy of tumor immunotherapy in aged mice. *Cancer Res.* **72**, 2089–2099 (2012).
39. D. K. Finch, R. Ettinger, J. L. Karnell, R. Herbst, M. A. Sleeman, Effects of CXCL13 inhibition on lymphoid follicles in models of autoimmune disease. *Eur. J. Clin. Invest.* **43**, 501–509 (2013).
40. Y. Wang *et al.*, Cytoplasmic DNA sensing by KU complex in aged $CD4^+$ T cell potentiates T cell activation and aging-related autoimmune inflammation. *Immunity* **54**, 632–647.e9 (2021).
41. J. Merkenschlager *et al.*, Dynamic regulation of T_{FH} selection during the germinal centre reaction. *Nature* **591**, 458–463 (2021).
42. M. A. Linterman *et al.*, IL-21 acts directly on B cells to regulate Bcl-6 expression and germinal center responses. *J. Exp. Med.* **207**, 353–363 (2010).
43. S. Goswami *et al.*, *ARID1A* mutation plus CXCL13 expression act as combinatorial biomarkers to predict responses to immune checkpoint therapy in mUCC. *Sci. Transl. Med.* **12**, eabc4220 (2020).
44. Q. Qi *et al.*, Diversity and clonal selection in the human T-cell repertoire. *Proc. Natl. Acad. Sci. U.S.A.* **111**, 13139–13144 (2014).
45. M. Ammirante, S. Shalapour, Y. Kang, C. A. Jamieson, M. Karin, Tissue injury and hypoxia promote malignant progression of prostate cancer by inducing CXCL13 expression in tumor myofibroblasts. *Proc. Natl. Acad. Sci. U.S.A.* **111**, 14776–14781 (2014).
46. A. B. Rodriguez *et al.*, Immune mechanisms orchestrate tertiary lymphoid structures in tumors via cancer-associated fibroblasts. *Cell Rep.* **36**, 109422 (2021).
47. L. D. Falo, Jr, M. Kovacsovics-Bankowski, K. Thompson, K. L. Rock, Targeting antigen into the phagocytic pathway in vivo induces protective tumour immunity. *Nat. Med.* **1**, 649–653 (1995).
48. H. Tsukamoto, Transcriptome analysis of whole lung tissue from anti-PD-1 therapy-treated mice. Gene Expression Omnibus. https://www.ncbi.nlm.nih.gov/geo/query/acc.cgi?acc=GSE184000. Deposited 30 May 2022.